

# **Title: Single shot ultrafast all optical magnetization switching of ferromagnetic Co/Pt multilayers**

**Authors:** Jon Gorchon<sup>1,2†</sup>, Charles-Henri Lambert<sup>2,†</sup>, Yang Yang<sup>3†</sup>, Akshay Pattabi<sup>2</sup>, Richard B. Wilson<sup>4</sup>, Sayeef Salahuddin<sup>1,2</sup>, Jeffrey Bokor<sup>1,2</sup>.

## **Affiliations:**

<sup>1</sup> Lawrence Berkeley National Laboratory, 1 Cyclotron Road, Berkeley, CA 94720, USA.

<sup>2</sup> Department of Electrical Engineering and Computer Sciences, University of California, Berkeley, CA 94720, USA.

<sup>3</sup> Department of Materials Science and Engineering, University of California, Berkeley, CA 94720, USA.

<sup>4</sup> Department of Mechanical Engineering and Materials Science and Engineering Program, University of California, Riverside, CA 92521, USA.

\*Correspondence to: jgorchon@lbl.gov, jbokor@berkeley.edu

†Denotes equal contribution.

## **Introduction:**

In a number of recent experiments<sup>1–8</sup>, it has been shown that femtosecond laser pulses can control magnetization on picosecond timescales, which is at least an order of magnitude faster compared to conventional magnetization dynamics. Among these demonstrations, one material system (GdFeCo ferromagnetic films) is particularly interesting, as deterministic toggle-switching of the magnetic order has been achieved without the need of any symmetry breaking magnetic field. This phenomenon is often referred to as all optical switching (AOS). However, so far, GdFeCo remains the only material system where such deterministic switching has been observed. When extended to ferromagnetic systems, which are of greater interest in many technological applications, only a partial effect can be achieved, which in turn requires repeated laser pulses for full switching<sup>9–11</sup>. However, such repeated pulsing is not only energy hungry, it also negates the speed advantage of AOS. Motivated by this problem, we have developed a general method for single-shot, picosecond timescale, complete all optical switching of

ferromagnetic materials. We demonstrate that in exchange-coupled layers of Co/Pt and GdFeCo, single shot, switching of the ferromagnetic Co/Pt layer is achieved within 7 picoseconds after irradiation by a femtosecond laser pulse. We believe that this approach will greatly expand the range of materials and applications for ultrafast magnetic switching.

### **Main text:**

Our model system consists of a perpendicularly magnetized ferromagnetic Co/Pt multilayer grown (see Methods) on a perpendicular GdFeCo layer (see Fig. 1a). The stacks were characterized by performing hysteresis loops with a magneto optical Kerr effect (MOKE) microscope (see Methods) and an out-of-plane magnetic field  $H_{\perp}$ . Hysteresis loops are shown in Fig.1b. Four remnant states are present in samples  $d=4$  and 5 nm, and only two in the strongly coupled  $d=1.5-3$  nm. We add a quarter wave plate in the optic path to enable depth-sensitive MOKE<sup>12</sup>, which allows us to obtain layer sensitivity, as demonstrated in the loops of Fig.1c. The polarity of the loops allows us to infer the directions of the magnetic moments in the stack (see Supp. Mat.). We indicate the direction of the Gd, FeCo and Co/Pt sublattice magnetizations by orange, green and blue arrows respectively. We note that the net moment of the GdFeCo/Co structures is dominated by the FeCo lattice (see Supp. Mat.).

Next, we characterize the type of the interlayer coupling of the stacks. We obtained the coupling for samples  $d=4$  and 5 nm by performing minor hysteresis loops, where only the Co/Pt magnetization is switched (blue circles in Fig.1b). The interlayer bias field  $H_b$  corresponds to the shift of the minor loop. The GdFeCo and Co/Pt net moments present an AFM coupling for thick spacers, as was found in Refs.<sup>13–15</sup>. An RKKY-type of exchange<sup>13–16</sup> or a dipolar orange peel coupling<sup>13,17</sup> could explain such AFM coupling. However, in Gd dominated samples,  $H_b$  has an

opposite sign (example shown in Supp. Mat. Fig.S3), demonstrating that the coupling does not follow the direction of the net moment, but rather the orientation of the sublattices. In addition, as shown by the magnetic moments depicted in Figs.1b and c, the coupling changes sign and becomes FM as the spacer is made thinner. We thus attribute the net coupling to an RKKY-type of exchange as reported in Refs.<sup>13–16</sup>.

We then check the all-optical switching capabilities of all the samples by irradiating the Co/Pt side (depicted in Fig.2a). MOKE micrographs of the AOS are shown in Fig.2b. The samples are initialized via a positive external magnetic field into a state where the GdFeCo and Co/Pt magnetizations are parallel. The magnetic field is then turned off. After the first single laser shot on sample  $d=5\text{nm}$  we observe two new regions of different contrast, a centered white circle and the surrounding grey ring (delimited by the white dashed line). The new regions present opposite anti-parallel alignments of GdFeCo and Co/Pt. In the center area, the laser intensity is above the critical fluence  $F_c$  for AOS, which results in the reversal of the GdFeCo magnetization. The Co/Pt magnetization remains in its initial orientation in order to relax the structure into a more stable AFM state. In the surrounding ring, the fluence is below threshold for AOS and GdFeCo does not switch. However, the hot Co/Pt layer does switch in order to relax into the AFM state. There is thus a second threshold  $F_c$  for the relaxation of the parallel state to antiparallel. For even lower fluences, the heating is insufficient to generate any observable changes. When the sample is shot with a second laser pulse, the magnetization in the center region switches fully, reversing both GdFeCo and Co/Pt moments. The ring region remains stable after the first shot, as it is already in a stable AFM state. We then repeat the experiment for different thicknesses  $d$  of the Pt spacer. Sample  $d=4\text{nm}$  presents the same type of switching as sample  $d=5\text{nm}$ . For samples

$d=1.5, 2$  and  $3$  nm, where the coupling is FM, we observe only the switching of the center area, as expected, as no more remnant states are available.

We illuminate the samples repeatedly and obtain reliable toggle switching of both ferromagnetic and ferrimagnetic layers for up to more than 100 pulses. The switching is reproducible in all FM and AFM coupled samples. This therefore presents the first demonstration of a single-shot AOS of a ferromagnetic film.

The absorbed critical fluences  $F_c$  for AOS, for relaxation as well as the estimated equilibrium lattice temperature rises  $\Delta T$  (see Supp. Mat.) are reported in Fig.2c by black, red and blue points, respectively. We obtain a temperature rise of  $\sim 150$  K for all films, irrespective of the type of coupling. The Co/Pt is thus heated to  $\sim 450$  K, very close to its expected Curie temperature of  $\sim 470$  K<sup>18</sup>. This indicates that for AOS to be possible the Co/Pt needs to be nearly fully demagnetized. Another possible mechanism to consider for switching are hot electron spin currents between the layers during demagnetization<sup>4</sup>. If present, spin currents should have a different sign for parallel and antiparallel alignments, resulting in different critical fluences. Because  $F_c$  for AOS is equal for AFM and FM coupled films, we believe that spin currents are probably not important to the switching mechanism.

The MOKE micrographs in Fig.2.b provide clear evidence of the AOS of Co/Pt, but cannot provide information on whether we are achieving ultrafast control over the exchange interaction, which is the ultimate goal of our study. In order to access the fast magnetization dynamics, we perform depth-sensitive time-resolved MOKE measurements<sup>19</sup> with no external magnetic field. Details of the technique are given in the Methods section. For this purpose, we grow a second series of two PMA samples with an extra Co/Pt repeat (Fig.3a), in order to increase the sensitivity to the Co/Pt layer. A patterned Au coil grown on top of the magnet was used to

deliver short intense magnetic field pulses at the laser repetition rate of 54 kHz to repetitively reset the magnetization between laser pulses during pump-probe experiments (see Methods). The Pt spacer thickness  $d$  of the samples was chosen equal to 1.5 and 4 nm, to obtain a strong FM and a weaker AFM coupling, respectively. We confirmed the AOS of the full stack in both samples by MOKE imaging.

We then perform low fluence demagnetization experiments in order to check the differences in demagnetization for a sample in an antiparallel (AP) vs a parallel (P) state. For this purpose, we work on sample  $d=4$  nm which has 4 remnant states. We first select the quarterwave plate angles in order to maximize layer sensitivity to the Co/Pt and GdFeCo moments, as shown in Fig.3b. By working at low fluence we avoid the full reversal of the Co/Pt layer, which has too high of a coercivity ( $\sim 500$  Oe) to be reset by the field delivered by the patterned coil. The results of the demagnetization dynamics are shown in Fig.3c. The Co/Pt and GdFeCo peak demagnetizations are similar in both parallel (P) and antiparallel (AP) cases, but the long timescale ( $\sim 2$ -20ps) dynamics of the Co/Pt magnetization are very different. We attribute the slower recovery of the parallel case to the intrinsic AFM coupling field of the stack that pulls the Co/Pt against the anisotropy field. If spin currents were relevant during demagnetization, they should be maximized during the fast demagnetization and have opposite signs for P and AP cases. The similar peak-demagnetization amplitudes for both P and AP cases indicate that spin currents do not play a major role.

Finally, we perform time-resolved switching experiments. Unfortunately, these experiments could not be carried on sample  $d=4$  nm because the coercivity of the Co/Pt layer is larger than the amplitude of the reset magnetic field we could generate with the patterned coils. We thus perform the AOS experiments on a thinner  $d=1.5$  nm sample, where both layers are strongly FM

coupled and present a single and smaller coercivity ( $H \sim 150$  Oe). We vary the incident average power from 40 to 59 mW.

As shown in Fig.3d, the dynamics of the GdFeCo and Co/Pt layers are quite different. At the lowest power, 40 mW, we only obtain a demagnetization of both GdFeCo and Co/Pt magnetizations. Increasing the power to 53 mW results in the switching of GdFeCo within  $\sim 3$  ps, during which the Co/Pt demagnetizes nearly completely. The magnetization of Co/Pt recovers during the next 4 ps as the system cools down. Eventually, due to the exchange field induced by the GdFeCo sublattice, the Co/Pt magnetization switches after  $\sim 30$  ps. At even high power, 59 mW, the Co/Pt demagnetizes first and then grows in the opposite direction, switching in only  $\sim 7$  ps.

The two-steps of the 7 ps switching event of Co/Pt shown in Fig.3d, - an initial full demagnetization and a subsequent switching - strongly supports the idea that the exchange interaction is responsible for the reversal of the softened (hot) Co/Pt magnetization. The curves at 53 and 59 mW indicate that the fastest switching occurs when the fluence is such that the temperature of the Co/Pt reaches exactly (or very close to)  $T_C$ , i.e a full demagnetization.

We have shown that, despite using thick (up to 5 nm) metallic Pt spacers to separate a Co/Pt multilayer from a GdFeCo layer, we can still achieve single-shot AOS of the ferromagnetic layer by exploiting the exchange interaction. Moreover, we demonstrated a 7 ps switching time on a sample with a 1.5 nm Pt spacer. This rather general method can be extended to other ferromagnets, ferrimagnets and even antiferromagnets. For example, the usage of high spin polarization materials coupled to GdFeCo should allow for ultrafast control of magnetic devices with high tunnel magneto resistance ratios<sup>20,21</sup>. In addition, such a method for ultrafast laser

writing of magnetic recording media without magnetic fields might be an appealing alternative for heat-assisted magnetic recording technology<sup>22</sup>. Finally, we believe that the combination of our approach with recent developments in ultrafast all-electronic switching of magnetism<sup>23</sup> enables additional new exciting possibilities for picosecond spintronics.

### **Acknowledgments:**

This work was primarily supported by the Director, Office of Science, Office of Basic Energy Sciences, Materials Sciences and Engineering Division, of the U.S. Department of Energy under Contract No. DE-AC02-05-CH11231 within the Nonequilibrium Magnetic Materials Program (MSMAG). We also acknowledge support by the National Science Foundation Center for Energy Efficient Electronics Science (materials synthesis, sample fabrication, and experimental equipment).

### **Author contributions:**

J.G., C.H.L, Y.Y and J.B devised the experiments. C.H.L grew the samples. Y.Y. did the microfabrication. J.G., C.H.L, Y.Y and A.P performed the experiments. J.G. wrote the manuscript with input from all the authors.

**The authors declare no competing financial interests.**

### **References and Notes:**

1. Stanciu, C. D. *et al.* All-optical magnetic recording with circularly polarized light. *Phys. Rev. Lett.* **99**, 47601 (2007).
2. Kirilyuk, A., Kimel, A. V & Rasing, T. Laser-induced magnetization dynamics and reversal in ferrimagnetic alloys. *Reports Prog. Phys.* **76**, 26501 (2013).
3. Beaurepaire, E., Merle, J.-C., Daunois, A. & Bigot, J.-Y. Ultrafast spin dynamics in ferromagnetic nickel. *Phys. Rev. Lett.* **76**, 4250–4253 (1996).
4. Malinowski, G. *et al.* Control of speed and efficiency of ultrafast demagnetization by

- direct transfer of spin angular momentum. *Nat. Phys.* **4**, 855–858 (2008).
5. Ostler, T. A. *et al.* Ultrafast heating as a sufficient stimulus for magnetization reversal in a ferrimagnet. *Nat. Commun.* **3**, 666 (2012).
  6. Choi, G.-M., Min, B.-C., Lee, K.-J. & Cahill, D. G. Spin current generated by thermally driven ultrafast demagnetization. *Nat. Commun.* **5**, 4334 (2014).
  7. Gorchon, J. *et al.* The role of electron temperature in the helicity-independent all-optical switching of GdFeCo. *Phys. Rev. B* **94**, 184406 (2016).
  8. Wilson, R. B. *et al.* Ultrafast magnetic switching of GdFeCo with electronic heat currents. *arXiv* 1609.05155 (2016).
  9. Lambert, C.-H. *et al.* All-optical control of ferromagnetic thin films and nanostructures. *Science* **345**, 1337–1340 (2014).
  10. El Hadri, M. S. *et al.* Two types of all-optical magnetization switching mechanisms using femtosecond laser pulses. *Phys. Rev. B* **94**, 64412 (2016).
  11. Takahashi, Y. K. *et al.* Accumulative magnetic switching of ultrahigh-density recording media by circularly polarized light. *Phys. Rev. Appl.* **6**, 54004 (2016).
  12. Schäfer, R. Magneto-optical domain studies in coupled magnetic multilayers. *J. Magn. Magn. Mater.* **148**, 226–231 (1995).
  13. Metaxas, P. J. *et al.* Magnetic domain wall creep in the presence of an effective interlayer coupling field. *J. Magn. Magn. Mater.* **320**, 2571–2575 (2008).
  14. Liu, Z. Y. *et al.* Oscillatory antiferromagnetic interlayer coupling in Co(4 Å)/Pt(t Å)/[Co(4 Å)/Pt(6 Å)/Co(4 Å)]NiO(20 Å) multilayers with perpendicular anisotropy. *Phys. Rev. B* **77**, 12409 (2008).
  15. Li, X. X., Bao, J., Lu, L. Y., Xu, X. G. & Jiang, Y. Oscillatory antiferromagnetic interlayer coupling in Co/Pt multilayer with perpendicular anisotropy. *Solid State Commun.* **148**, 209–212 (2008).
  16. Bersweiler, M., Lacour, D., Dumesnil, K., Montaigne, F. & Hehn, M. Phase diagram in exchange-coupled CoTb/[Co/Pt] multilayer-based magnetic tunnel junctions. *Phys. Rev. B* **92**, 224431 (2015).
  17. Moritz, J., Garcia, F., Toussaint, J. C., Dieny, B. & Nozieres, J. P. Orange peel coupling in multilayers with perpendicular magnetic anisotropy : Application to ( Co / Pt ) -based. *Europhys. Lett.* **65**, 123–129 (2004).
  18. Metaxas, P. J. *et al.* Creep and flow regimes of magnetic domain-wall motion in ultrathin Pt/Co/Pt films with perpendicular anisotropy. *Phys. Rev. Lett.* **99**, 217208 (2007).
  19. Schellekens, A. J., de Vries, N., Lucassen, J. & Koopmans, B. Exploring laser-induced interlayer spin transfer by an all-optical method. *Phys. Rev. B* **90**, 104429 (2014).
  20. Nishimura, N. *et al.* Magnetic tunnel junction device with perpendicular magnetization films for high- density magnetic random access memory. *J. Appl. Phys.* **91**, 5246–5249 (2002).
  21. Chen, J., He, L., Wang, J. & Li, M. Picosecond all-optical switching of magnetic tunnel



- junctions. *arXiv* 1607.04615 (2016).
22. Thiele, J.-U., Coffey, K. R., Toney, M. F., Hedstrom, J. A. & Kellock, A. J. Temperature dependent magnetic properties of highly chemically ordered Fe(55-x)Ni(x)Pt(45)L1(0) films. *J. Appl. Phys.* **91**, 6595 (2002).
  23. Yang, Y. *et al.* Ultrafast Magnetization Reversal by Picosecond Electrical Pulses. *arXiv* 1609.06392 (2016).

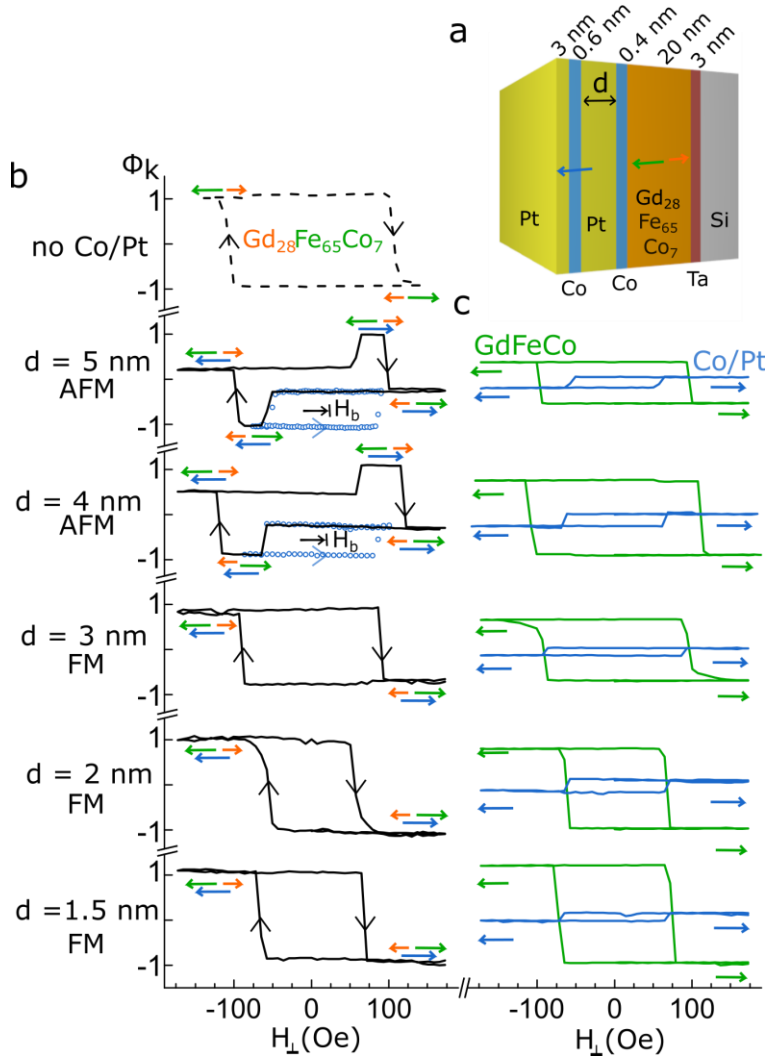


**Fig. 1. Sample description and magnetic characterization.** **a**, GdFeCo/Co/Pt(d nm)/Co stack series with Pt spacer of thickness d. **b**, Magnetic hysteresis loops for (top) bare GdFeCo(20 nm)/Ta(3 nm) and the GdFeCo/Co/Pt/Co stacks with different Pt spacer. Green, orange and blue

arrows represent Gd, FeCo and Co/Pt magnetizations, respectively. Minor loops switching only the Co/Pt magnetization, presenting a positive exchange bias  $H_b$ , on samples  $d=4$  and 5 nm. **c**, Depth sensitive MOKE hysteresis loops of the stacks, with maximum sensitivity to GdFeCo (green) and Co/Pt (blue) magnetic lattices.

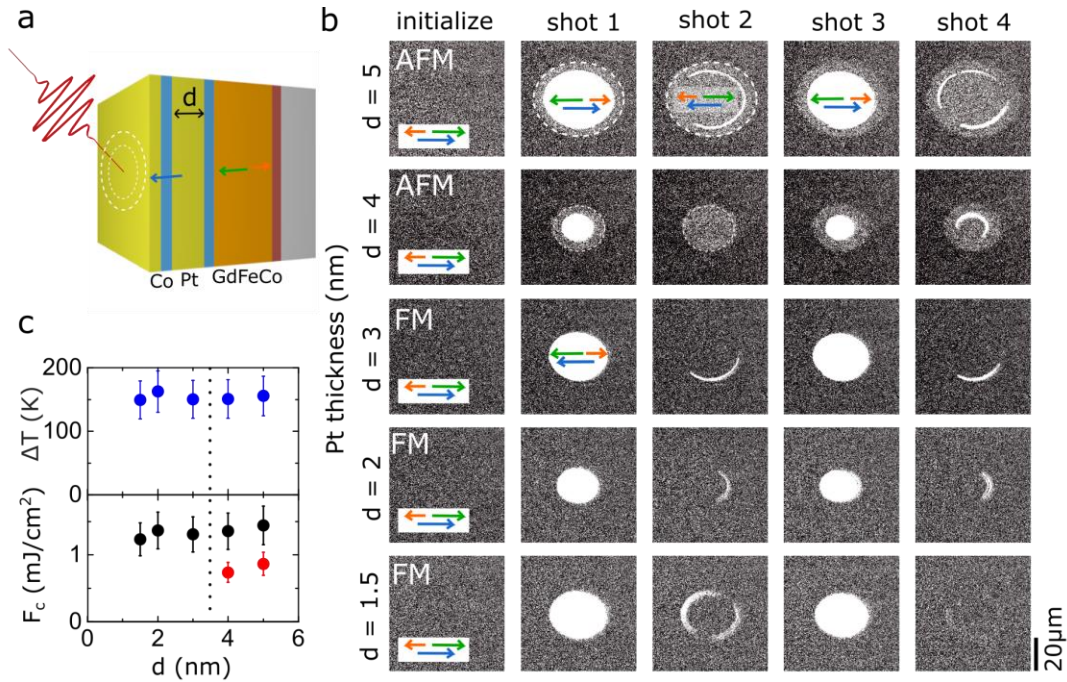


**Fig. 2. Single shot all optical switching of both Co/Pt and GdFeCo layers.** **a**, Schematic of experiment with GdFeCo/Co/Pt( $d$  nm)/Co stack series presented in Fig.1 **b**, MOKE images of a sequence of AOS events on films with different Pt spacers. Green, orange and blue arrows represent Gd, FeCo and Co/Pt magnetizations, respectively. **c**, Absorbed critical fluence  $F_c$  for AOS (in black),  $F_c$  for relaxation of parallel states (in red), corresponding to the dotted lines in

Fig.2b, and estimated peak lattice temperature rises  $\Delta T$  (in blue) as a function of the Pt spacer thickness.

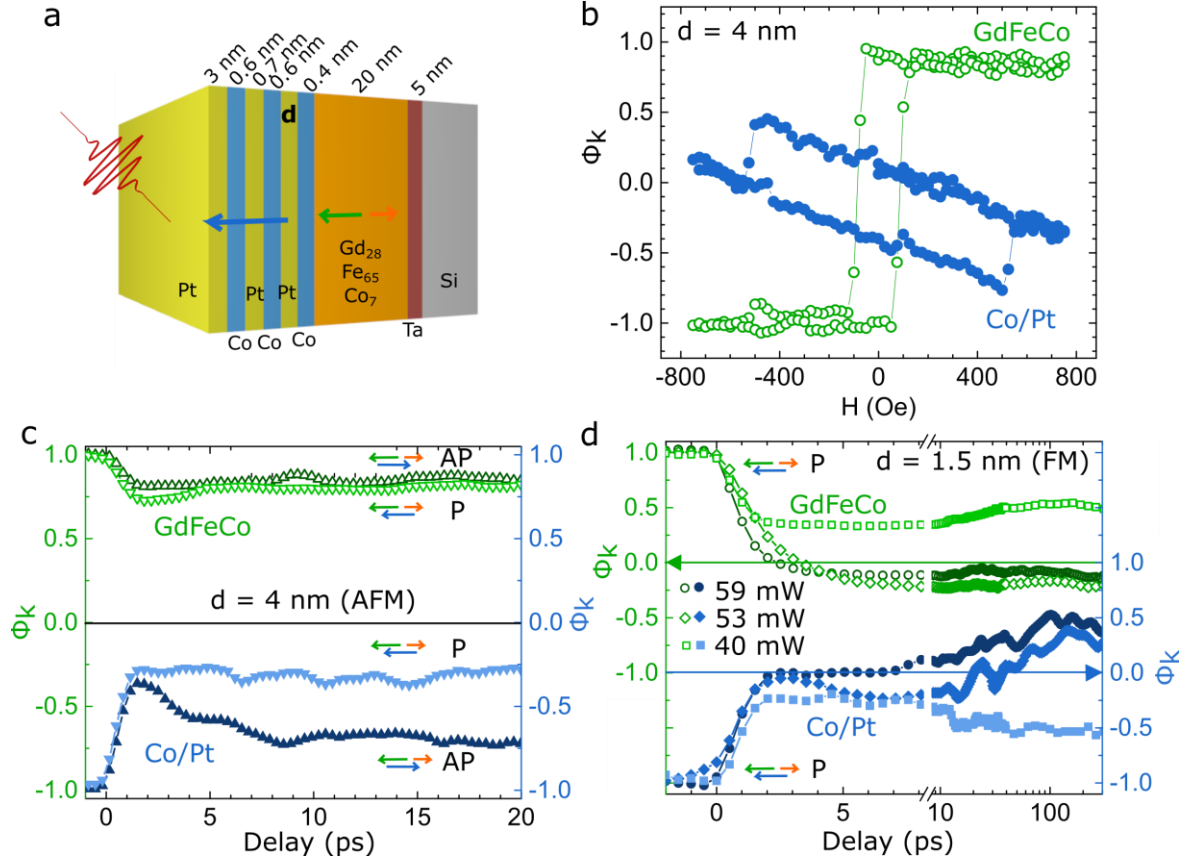


**Fig. 3. Time-resolved depth-sensitive magneto-optical measurements of laser induced dynamics.** **a**, GdFeCo/Co/Pt(d nm)/[Co/Pt]<sub>2</sub> stack series with Pt spacer of thickness d. **b**, Depth-sensitive MOKE magnetic hysteresis loops on sample d=4 nm. **c**, Depth-sensitive time-resolved demagnetization curves for antiparallel (AP) or parallel (P) initial states of the stack d=4 nm. Green, orange and blue arrows represent Gd, FeCo and Co/Pt magnetizations, respectively. **d**, Depth-sensitive demagnetization and AOS experiments at various fluences on sample d=1.5 nm.

# Supplementary Materials for

## Single shot ultrafast all optical magnetization switching of ferromagnetic Co/Pt multilayers

Jon Gorchon, Charles-Henri Lambert, Yang Yang, Akshay Pattabi, Richard B. Wilson, Sayeef Salahuddin, Jeffrey Bokor

correspondence to: [jgorchon@lbl.gov](mailto:jgorchon@lbl.gov)

### **This PDF file includes:**

Materials and Methods  
SupplementaryText  
Figs. S1 to S5  
Table S1

## Materials and Methods

### Samples:

We grew two different series of stacks by magnetron sputter deposition on Si/SiO<sub>2</sub>(100 nm) substrates. The stacks, as shown in Figures 1.a and 3a, are Ta(3 nm)/GdFeCo(20 nm)/Co(0.4 nm)/Pt(d)/Co(0.6 nm)/Pt(3 nm), Ta(5 nm)/GdFeCo(20 nm)/Co(0.4 nm)/Pt(d)/Co(0.6 nm)/Pt(0.7 nm)/Co(0.6 nm)/Pt(3 nm). The spacer thickness d was varied between 0 and 5 nm. The layer thicknesses were determined from the deposition rate of each material. All of the samples presented perpendicular magnetic anisotropy (PMA). The compensation temperature  $T_m$ , temperature at which the magnetic moment is minimized, determines the dominant magnetic moment, FeCo for  $T_m < 300$  K, and Gd for  $T_m > 300$  K.

### Experimental setups:

The experimental setups consist of a magneto-optical microscope shown in Fig.S1 and a time-resolved magneto-optical laser setup shown in Fig.S2. In both setups we irradiated the samples with 70 fs (FWHM) laser pulses of 810 nm center-wavelength incident at a 40° angle to normal. The microscope (Fig.S1) exploits the magneto-optical Kerr effect (MOKE) with a 630 nm light-emitting diode (LED) source to image the magnetization of the samples. The laser setup (Fig.S2) uses an 810 nm center-wavelength laser probe beam brought in at normal incidence to probe the magnetization in a classical pump-probe configuration. Both, 630 nm and 810 nm light probes are mostly sensitive to the magnetization of FeCo sublattice within the 20 nm of GdFeCo<sup>2</sup>. We also detect a weaker Kerr signal originating from the thin Co/Pt multilayers. A quarter-wave plate (QWP) after the polarizer in the MOKE microscopy setup allows to mix the Kerr ellipticity and rotation signals and obtain *depth-sensitive* MOKE<sup>12</sup>. Changing the angle of the quarter wave plate allows for a tuning of the amplitude of the Kerr signal originating from each layer, up to complete extinction of the Kerr signal of either one of the layers, as shown in Fig.1D. Similarly, a QWP in the laser setup enables depth-sensitive time-resolved MOKE<sup>19</sup>. More details on this technique are given in the Supplementary Materials.

## Supplementary Materials

### Depth-sensitive time-resolved MOKE with no constant magnetic field:

A schematic of the setup is shown in Fig.S.2. To measure the small polarization rotation in the laser probe induced by MOKE, a photo-elastic modulator (PEM) and lock-in detection is used. The PEM modulates the polarization of the probe beam at 50 kHz. After the reflection off the sample, the probe beam goes through an analyzer, converting polarization changes into intensity changes. The intensity of the probe beam is then measured with a Si photo-detector (Thorlabs PDB 450A-AC). By sending this intensity signal into a lock-in amplifier referenced at the PEM frequency (twice the PEM frequency), the rotation (ellipticity) of the polarization caused by the magnetization can be obtained. We add a quarter-wave plate (QWP) before the PEM, and by rotating its angle, a signal proportional to a mix of Kerr ellipticity and rotation is measured. At specific QWP angles, Kerr ellipticity and rotation cancel each other so that we can

annihilate the magnetic response from a specific layer. For more details, refer to Ref.19. In the following, we will probe analytically how the QWP modifies the sensitivity:

The incoming light is  $45^\circ$  linearly polarized, so it can be written as  $\begin{pmatrix} 1 \\ 1 \end{pmatrix}$  in Jones matrix formalism. The Jones matrices for the rest of the optical system, the QWP, PEM, Kerr rotation, Kerr ellipticity and analyzer (A) can be written as,

$$QWP = \begin{pmatrix} \cos \alpha & \sin \alpha \\ -\sin \alpha & \cos \alpha \end{pmatrix} \cdot \begin{pmatrix} 1 & 0 \\ 0 & i \end{pmatrix} \cdot \begin{pmatrix} \cos \alpha & -\sin \alpha \\ \sin \alpha & \cos \alpha \end{pmatrix}$$

$$PEM = \begin{pmatrix} 1 & 0 \\ 0 & e^{-i\beta \sin(\omega t)} \end{pmatrix}$$

$$Kerr_{rot} = \begin{pmatrix} \cos \theta & -\sin \theta \\ \sin \theta & \cos \theta \end{pmatrix}$$

$$Kerr_{el} = \begin{pmatrix} 1 & -i * \epsilon \\ i * \epsilon & 1 \end{pmatrix}$$

$$A = \begin{pmatrix} 0 & 0 \\ 0 & 1 \end{pmatrix}$$

where  $\alpha, \omega, \beta, \theta, \epsilon$  are the angle of fast axis of quarter-wave plate (with respect to horizontal plane), the frequency of PEM, the amplitude of modulation of the phase (a.k.a retardation) by the PEM, the Kerr rotation and the Kerr ellipticity, respectively.

By multiplying the matrices with the initial polarization state, the final  $2\omega$  signal ( $V_{2\omega}$ ) obtained on the lock-in amplifier is,

$$V_{2\omega} \propto \theta * (\sin 2\alpha)^2 + \epsilon * \cos 2\alpha$$

As the Kerr rotation and ellipticity are proportional to the magnetization  $M$ , we can write,

$$V_{2\omega} \propto M[\theta' * (\sin 2\alpha)^2 + \epsilon' * \cos 2\alpha]$$

By choosing the right angle  $\alpha$  of the quarter-wave plate, any linear combination of  $\theta'$  and  $\epsilon'$  can be obtained. Specifically, there always exist an angle  $\alpha$  such that the  $2\omega$  signal remains zero, and the magnetic response is annihilated. Since the Kerr rotation and ellipticity are additive, the total rotation and ellipticity of a magnetic bilayer corresponds to  $\theta_T = \theta_1 + \theta_2$  and  $\epsilon_T = \epsilon_1 + \epsilon_2$  respectively where  $\theta_1, \theta_2, \epsilon_1$  and  $\epsilon_2$  are the rotations and ellipticities of layer 1 and 2. The  $2\omega$  total signal ( $V_{2\omega,T}$ ) obtained on the lock-in amplifier is thus a sum of the signals due to each layer:  $V_{2\omega,T} = V_{2\omega,1} + V_{2\omega,2}$ . The sensitivity to each layer can be tuned with the QWP angle as shown in Fig.S3. We can therefore, select an angle of the QWP so that the signal from one layer is completely eliminated ( $\sim 102^\circ$  and  $\sim 120^\circ$  on Fig.S3), independently of its magnetization.

Finally, in a pump-probe configuration (Fig.S.2), where the pump and the probe beams are delayed via a mechanical stage (delay line), we can probe pump induced changes on the magnetization of one single layer within the bilayer.

Due to the stroboscopic nature of pump-probe experiments, the magnetization of both layers needs to be reset after each laser pulse. For this purpose, we patterned small 300 nm thick Au coils on top of the films (see inset in Fig.S.2) in order to deliver short intense magnetic field pulses in between pump pulses, and avoid any constant external field that could affect the magnetization dynamics. We performed the experiment at 54 kHz and used 2  $\mu$ s wide electrical pulses of 1 A in amplitude generated by an amplified waveform generator. The electrical pulses were synchronized via a delay generator which was triggered by a photodiode within the laser cavity. The 54 kHz repetition rate allows for  $\sim 16 \mu$ s of cooling time for the sample after the optical and electrical pulses, so that the initial state is always in equilibrium and at room temperature. All time-resolved curves in Fig.4 were obtained by performing the experiment for positive and negative magnetizations and taking the difference of the two signals in order to eliminate non-magnetic contributions to the signal.

#### Magnetic moment characterization:

The analysis carried on all the samples will be explained in the following, by taking the example of the samples presented in Fig1. First, a hysteresis of the bare film Gd<sub>28</sub>FeCo(20 nm)/Ta(3 nm) is obtained (top hysteresis in Fig.1.C), which indicates that the compensation temperature is below room temperature. This conclusion is achieved by comparing the polarity of the hysteresis to previously characterized samples in Refs.7. The dominant magnetic moment in the ferrimagnet is thus the FeCo moment at room temperature. We conclude that the highest coercivity ( $\sim 100$  Oe) in the weakly coupled stacks is given by the GdFeCo layer, by comparing the direction of the coercive jumps (in other words, we compare the polarity of the hysteresis). Moreover, this is confirmed by the large Kerr signal (bigger jump) which we attribute to the thicker (20 nm) FeCo lattice.

Depth-sensitive MOKE was used to slightly increase the sensitivity to the thin Co/Pt layer and obtain the hysteresis reported in Figs.1C, 3C and 3D. Single layer sensitivity is demonstrated in the top hysteresis loops of Fig.1.E, where distinct coercivities for each layer are distinguishable. We then fix the quarter wave plate at an angle, maximizing sensitivity to either layer, and perform hysteresis loops on all the samples. We repeat the experiment with a second angle of the quarter wave plate that provides high sensitivity to the other layer. These hysteresis loops are reported in Fig.1E. We assume that the sensitivity to a single layer remains valid as the thickness of the spacer changes, as a non-magnetic spacer should not influence the complex Kerr signal. From the polarity of the cycles we extract the relative magnetization direction of the probed lattice.

#### Absorption calculation:

For the multilayer calculation, the index of refraction and thickness reported in Table S1 were used. The electric field inside the stack was obtained through the matrix transfer method. The absorption was then obtained by calculating the divergence of the Poynting vector inside the stack. The obtained absorption per layer for a beam incident at 40 degrees to normal, with s-polarization, for the case of a Pt thickness of  $d=5$  nm is reported in Table 1, and the absorption profile is shown in Fig.S4. The total absorption of the stack was around  $\sim 33\%$ .

#### Temperature rise calculation:

The transient equilibrium temperature rise for the whole stack is calculated by the following formula:

$$\Delta T = \frac{F_c}{C \cdot t}$$

Where  $F_c$  is the absorbed critical fluence,  $C \sim 2.9 \text{ MJ}/(\text{Km}^3)$  is the weighted heat capacity of the full stack (using the heat capacity of GdFeCo of  $3 \text{ MJ}/(\text{Km}^3)$  from Ref.7), and  $t$  is the total thickness of the stack.



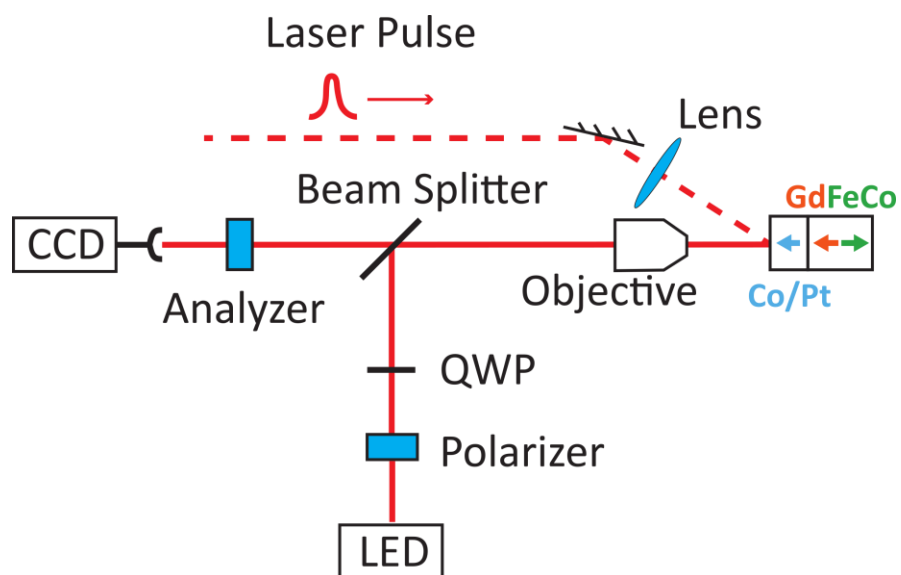


**Fig. S1.**

Depth-sensitive magneto-optical Kerr effect microscope setup.

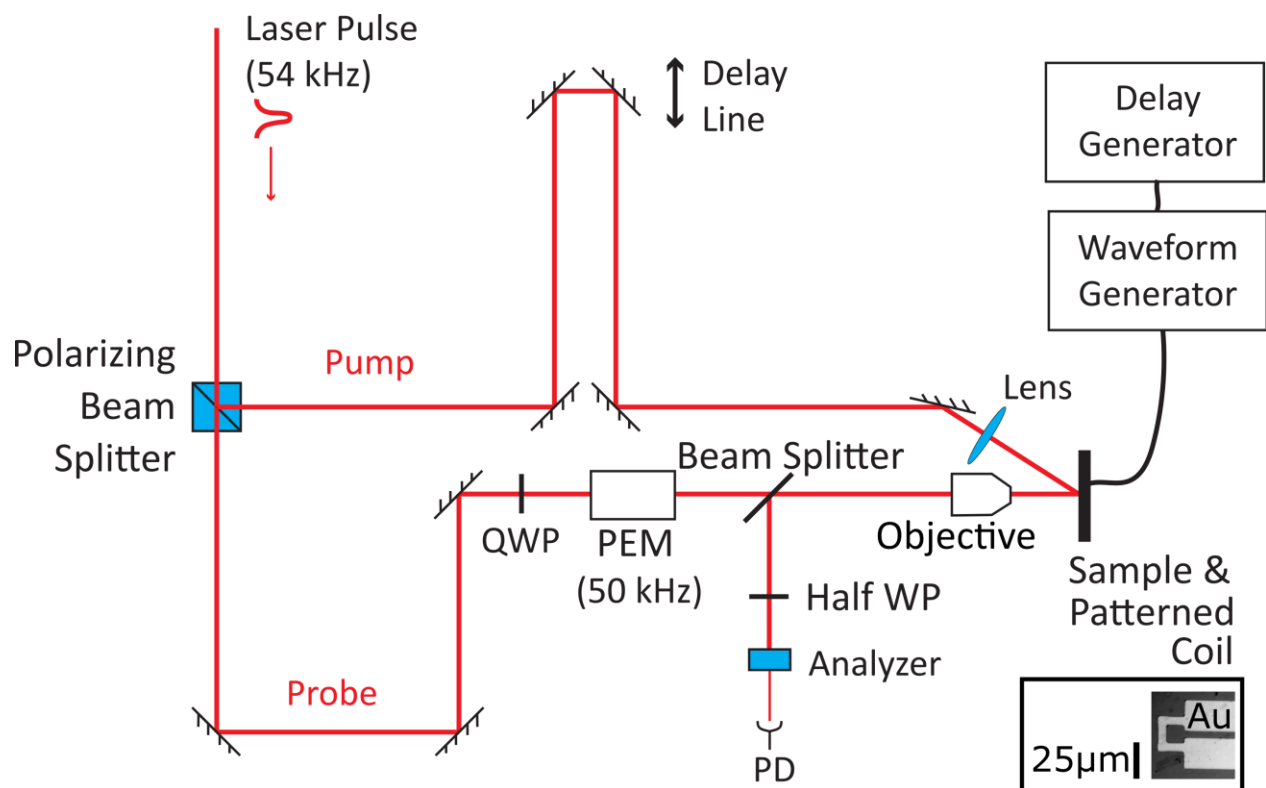


**Fig. S2.**

Depth-sensitive magneto-optical Kerr effect time-resolved setup.

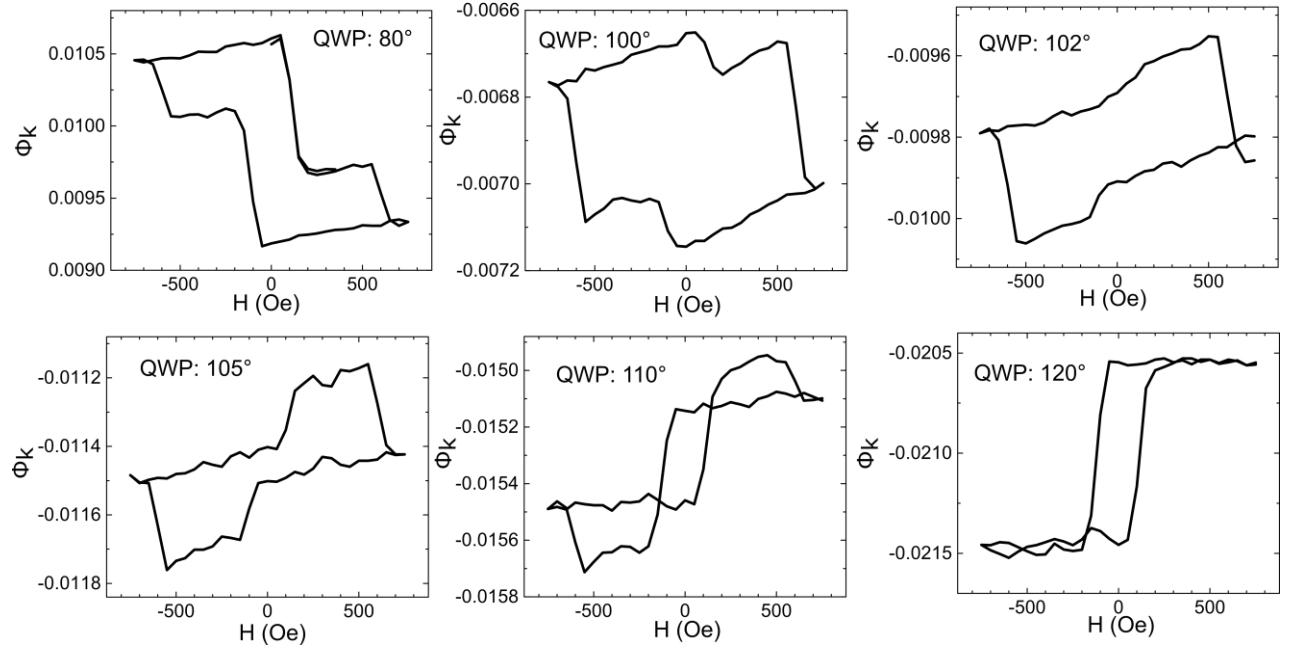


**Fig. S3.**

Depth-sensitive laser magneto-optical Kerr effect hysteresis loops vs quarter-wave plate (QWP) angle, on sample GdFeCo/Co/Pt(4nm)/[Co/Pt]/Co/Pt from Fig.2.A.

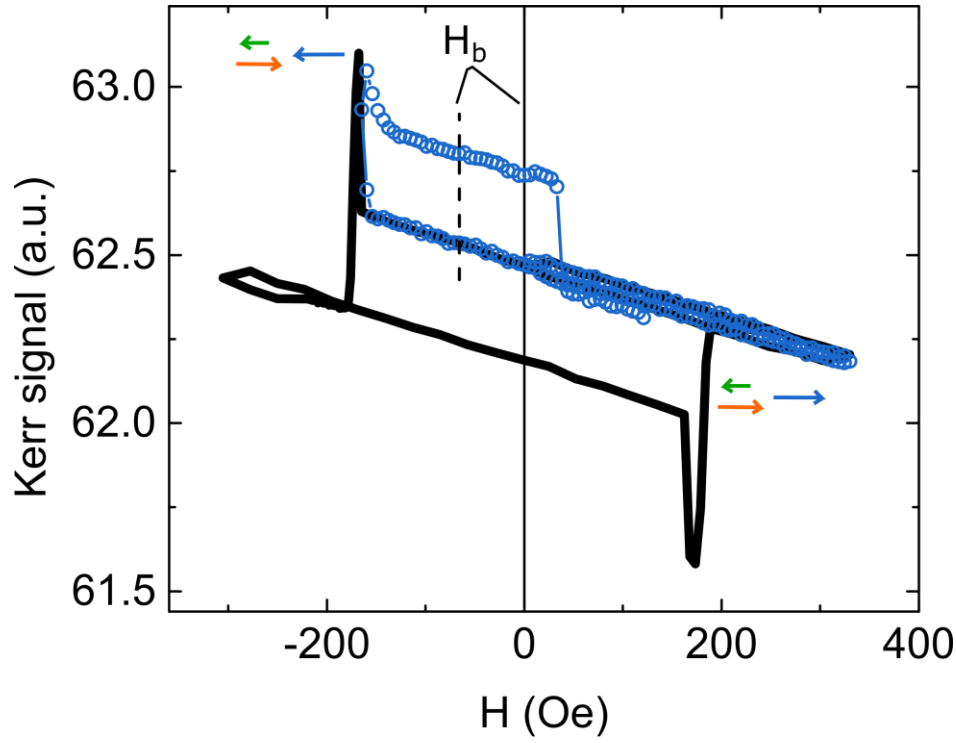


**Fig. S4.**

Minor hysteresis loop of the Co/Pt layer in a Gd rich Si/SiO<sub>2</sub>(100nm)/Ta(5nm)/(Gd<sub>36</sub>Fe<sub>57.6</sub>Co<sub>6.4</sub>)(20 nm)/Pt(4.1nm)/Co(1.2nm)/Pt(5nm) sample. Blue, green and orange arrows represent Co/Pt, FeCo and Gd magnetizations. Note the opposite sign of the exchange bias  $H_b$  shift with respect to the one observed in FeCo rich samples (Fig.1E). The Co/Pt layer is thus coupled with the sublattices instead of the net moment, just as expected for interlayer exchange coupling.

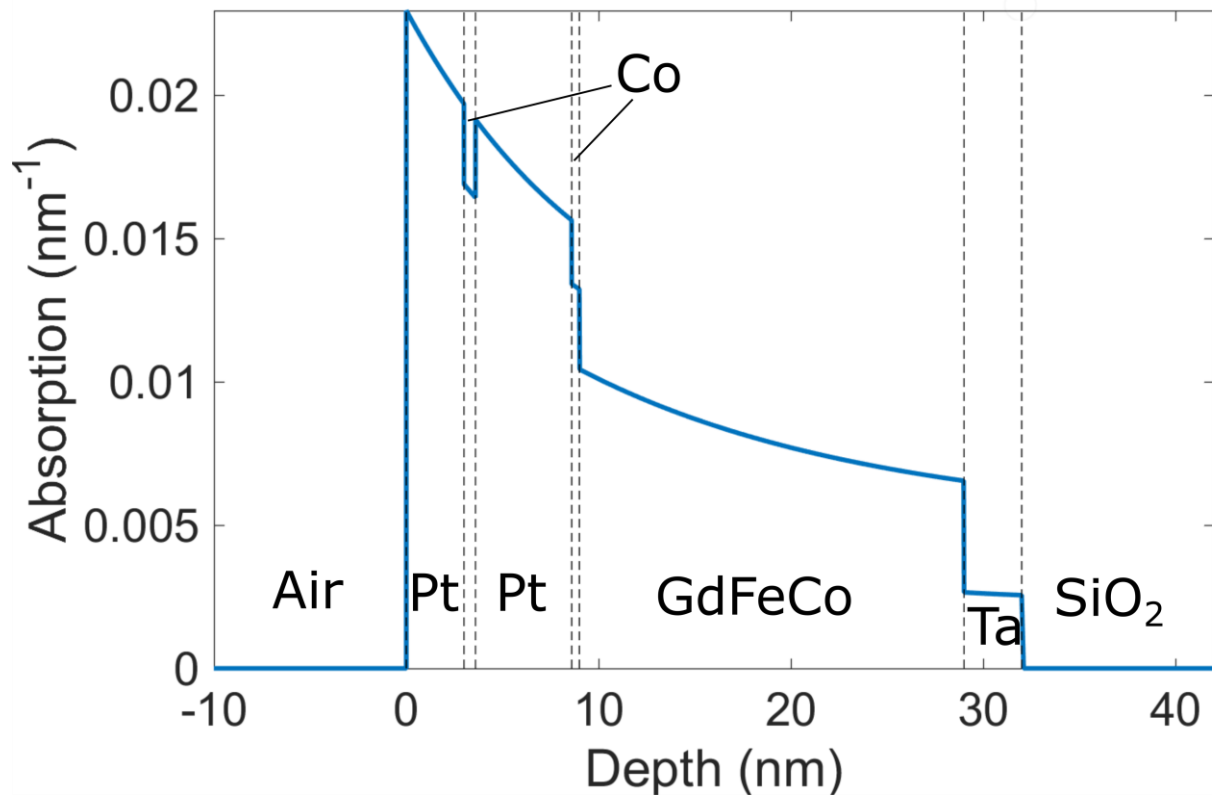


**Fig. S5.**

Absorption profile for the GdFeCo/Co/Pt(5nm)/Co/Pt stack from Fig.1.

Layer	Thickness (nm)	Complex index of refraction	Absorption by layer (%)
air	-	1	-
Pt	3	$2.85 + 4.96i$	6.4
Co	0.6	$2.50 + 4.84i$	1.0
Pt	5	$2.85 + 4.96i$	8.6
Co	0.4	$2.50 + 4.84i$	0.5
GdFeCo	20	$2.66 + 3.56i$	16
Ta	3	$1.09 + 3.06i$	0.8
SiO <sub>2</sub>	100	1.45	0
Si	-	$3.70 + 0.005i$	-

**Table. S1.**

Multilayer calculation parameters and absorption per layer. All refractive indexes were obtained from <http://refractiveindex.info> (references provided). The refractive index of GdFeCo at 800nm was obtained from Ref.2. Using the slightly different index of refraction for GdFeCo from Ref.7 did not change substantially the total absorption.